RESEARCH ARTICLE

Phytophthora effector PSR1 hijacks the host pre-mRNA splicing machinery to modulate small RNA biogenesis and plant immunity

Xinmeng Gui^{1, 7}, Peng Zhang^{1, 2, 7}, Dan Wang^{1, 7}, Zhan Ding^{3, 4, 7}, Xian Wu¹, Jinxia Shi¹, Qian-Hua Shen⁵, Yong-Zhen Xu^{3, 4}, Wenbo Ma⁶, Yongli Qiao^{1*}

Short title: PINP1 functions in sRNA and plant immunity

One-sentence summary: PSR1 affects the ability of PINP1 in binding to pri-miRNAs and the alternative pre-mRNA splicing in plants, thereby impeding sRNA biogenesis and plant immunity.

The author responsible for distribution of materials integral to the findings presented in this article in accordance with the policy described in the Instructions for Authors (https://academic.oup.com/plcell) is Yongli Qiao (qyl588@gmail.com).

ABSTRACT

Phytophthora effector PSR1 suppresses small RNA (sRNA)-mediated immunity in plants, but the underlying mechanism remains unknown. Here, we show that Phytophthora suppressor of RNA silencing 1 (PSR1) contributes to the pathogenicity of Phytophthora sojae and specifically binds to three conserved C-terminal domains of the eukaryotic PSR1-Interacting Protein 1 (PINP1). PINP1 encodes PRP16, a core pre-mRNA splicing factor that unwinds RNA duplexes and binds to primary microRNA transcripts (pri-miRNAs) and general RNAs. Intriguingly, PSR1 decreased both RNA helicase and RNA-binding activity of PINP1, thereby dampening sRNA biogenesis and RNA metabolism. The PSR1-PINP1 interaction caused global changes in alternative splicing (AS). A total of 5,135 genes simultaneously exhibited mis-splicing in both PSR1-overexpressing and PINP1-silenced plants. AS upregulated many mRNA transcripts that had their introns retained. The high occurrence of intron-retention (IR) in AS-induced transcripts significantly promoted Phytophthora pathogen infection in Nicotiana benthamiana, and this might be caused by the production of truncated proteins. Taken together, our findings reveal a key role for PINP1 in regulating sRNA biogenesis and plant immunity.

¹ Shanghai Key Laboratory of Plant Molecular Sciences, College of Life Sciences, Shanghai Normal University, Shanghai, 200234, China

² College of Agriculture, Yangtze University, Jingzhou, 434025, China

³ Key Laboratory of Insect Developmental and Evolutionary Biology, CAS Center for Excellence in Molecular Plant Sciences, Shanghai Institute of Plant Physiology and Ecology, Chinese Academy of Sciences, Shanghai, 200032, China

⁴ State Key Laboratory of Virology, Hubei Key Laboratory of Cell Homeostasis, College of Life Science, Wuhan University, Hubei, 430072, China

⁵ State Key Laboratory of Plant Cell and Chromosome Engineering, Institute of Genetics and Developmental Biology, Chinese Academy of Sciences, Innovation Academy for Seed Design, Beijing 100101, China

⁶ The Sainsbury Laboratory, Norwich Research Park, Norwich, NR4 7UH, UK

⁷ These authors contributed equally to this work.

^{*}Author for correspondence: Yongli Qiao, qyl588@gmail.com

INTRODUCTION

Posttranscriptional regulation of gene expression plays a crucial role in diverse cellular processes such as development, metabolism and cancer progression. RNA splicing processes pre-mRNA transcripts by first removing introns from nascent RNA transcripts and subsequently joining exons together (Nasif et al., 2018). Alternative splicing (AS) of RNAs is a critical process that produces multiple transcripts from a single gene, promoting genetic diversity and complexity. Recent studies indicate that approximately 95% of human and 60% of plant multiexonic genes exhibit AS (Pan et al., 2008; Marquez et al., 2012). Five different types of AS events have been reported to date including intron retention (IR), exon skipping (ES), mutually exclusive exons (MXEs), alternative 5' splice sites (A5SSs), and alternative 3' splice sites (A3SSs), and plant AS exhibits remarkable differences compared with metazoan AS. IR is the most prevalent AS event in plants, whereas ES is the most common AS event in animals (Reddy et al., 2013).

IR occurs when an intron is not spliced out, leading to a newly mature mRNA containing an unprocessed sequence. IR frequently results in frame shift mutations and/or introduction of a premature termination codon (PTC), and the resulting transcripts are either exported to the cytoplasm for degradation via the nonsense-mediated RNA decay (NMD) pathway or targeted by the nuclear RNA surveillance machinery prior to export (Wong et al., 2013). Nevertheless, little is known about the mechanisms driving AS.

Many human diseases, such as Becker muscular dystrophy, dilated cardiomyopathy, and early-onset Parkinson's disease, are closely related to splicing defects or are triggered by splicing mis-regulation (Scotti and Swanson, 2016). The splicing reactions are catalyzed by large protein–RNA complexes called spliceosomes, which are composed of five small nuclear RNAs (snRNAs; U1, U2, U4, U5, and U6) and several associated proteins (Wilkinson et al., 2020). Multiple conformational and compositional changes in the spliceosome are driven by eight superfamily 2 (SF2) helicases. These helicases are categorized into three families (DEAD-box, DEAH-box, and Ski2-like), based on sequence homology as well as similar functional and structural characteristics (De Bortoli et al., 2021). Four spliceosomal helicases, including three DEAD-box subfamily helicases (PRP5, UAP56, and PRP28) and one Ski2-like subfamily helicase (Brr2), are involved in the early steps of spliceosome assembly and activation. Four additional DEAH-box subfamily helicases (PRP2, PRP16, PRP22, and PRP43) act during the catalysis and

disassembly stages of the splicing cycle (De Bortoli et al., 2021). However, the biological functions and biochemical activities of these helicases remain poorly characterized in plants.

AS has been widely investigated in plants, and is involved in regulating diverse physiological processes, such as plant development, hormone biosynthesis, and stress response (Rigo et al., 2019). The precise splicing of defense-related transcripts is necessary to regulate disease resistance in plants (Zhang and Gassmann, 2003; Yang et al., 2008; Xu et al., 2012; Zhang et al., 2014). However, the molecular mechanism that underlies AS-mediated regulation of plantmicrobe interactions remains largely unknown. Recent studies show that HopU1, a bacterial type III effector from *Pseudomonas syringae*, represses plant immunity by binding to plant GRP7, an RNA-binding protein that modulates the AS of certain transcripts via direct interaction with target mRNAs (Streitner et al., 2012). The *Phytophthora sojae* effector PsAvr3c interacts with soybean (Glycine max) Ser/Lys/Arg-rich proteins (GmSKRPs) to inhibit proteasomal degradation and promote disease. GmSKRPs interact with key spliceosome components, thus disrupting host RNA splicing (Huang et al., 2017). The Phytophthora infestans effector SRE3 physically interacts with the spliceosomal U1-70K protein and splicing regulatory proteins (SR30 and SR45) to manipulate the AS of host pre-mRNAs and suppress plant immunity (Huang et al., 2020). In addition, the cyst nematode effector 30D08 directly interacts with SMU2, an auxiliary spliceosomal protein, to manipulate host cellular processes and establish the feeding site (Verma et al., 2018). These studies indicate that AS regulation is important for plant immunity, and how pathogens have evolved effectors that target the host splicing components to promote disease. However, the regulatory programs involved in these AS processes, coupled with the NMD pathway, in plants is not well defined.

Phytophthora root rot, caused by *P. sojae*, is one of the most serious soil-borne diseases in soybean-production regions worldwide (Ma et al., 2017). We previously showed that the *P. sojae* effector PSR1 facilitates infection by inhibiting small RNA (sRNA) biogenesis in plants (Qiao et al., 2013; Shi et al., 2020), and that the WY domain of PSR1 is essential for *P. sojae* infection and RNA silencing suppression activity (Zhang et al., 2019). PSR1 regulates sRNA accumulation and plant development by associating specifically with PINP1, which is also known as premRNA splicing factor 16 (PRP16), to promote disease in *Arabidopsis thaliana*, *N. benthamiana*, and *Glycine max* (Qiao et al., 2015). PINP1 belongs to the MUT6 family of proteins, which

contain the DEAH-box RNA helicase domain (Linder and Owttrim, 2009). In *Chlamydomonas*, MUT6 is required for the silencing of transgenes and transposons, and is involved in RNA turnover (Wu-Scharf et al., 2000). In animals, the DEAD-box RNA helicase DDX17 binds to the stem-loop structure of primary microRNAs (pri-miRNAs) and facilitates their processing (Moy et al., 2014). The SDE3 family of DEAD-box RNA helicases associates with ARGONAUTEs and promotes the production of secondary small interfering RNAs (siRNAs) in plants and animals (Garcia et al., 2012). Both DDX17 and SDE3 are required for antiviral immunity. However, the molecular mechanisms underlying the regulation of sRNA biogenesis and plant immunity by PINP1 remain unknown.

Here, we report that PSR1 specifically binds to the evolutionarily conserved PINP1 homologs. PINP1 possesses both RNA helicase and RNA-binding activities, and functions in pre-mRNA splicing. PINP1 binds to the stem-loop structure of pri-miRNAs and facilitates sRNA biogenesis. Silencing of PINP1 results in global changes in AS, particularly IR, in plants, and PINP1 silencing affects the expression of many genes and increases the occurrence of IR in mRNA transcripts. Importantly, we demonstrate that the PSR1–PINP1 interaction dampens PINP1 functions, thereby resulting in massive PINP1-mediated AS events and impeding the efficient processing of PINP1 target transcripts involved in sRNA biogenesis and plant immunity.

RESULTS

PSR1 contributes to the pathogenicity of *P. sojae* and binds to PINP1 homologs in plants, animals, and microbes

Previous studies suggest that PSR1 facilitates the infection of *Arabidopsis*, *N. benthamiana*, and soybean by *Phytophthora* spp. and viruses (Qiao et al., 2013; Zhang et al., 2019). To further determine its contribution to *P. sojae* virulence, we generated three *PSR1*-edited *P. sojae* mutants using the CRISPR/Cas9 system (Supplemental Figure 1A, 1B). Compared with the wild-type (WT) strain, three *PSR1*-edited transformants (T3, T20, T22) showed no developmental defects (Figure 1A, Supplemental Figure 1C–1D). However, all three *PSR1*-edited mutants caused smaller lesions and produced considerably lower biomass on soybean seedlings than the WT strain (Figure 1A and 1B). This indicates that PSR1 is crucial for the virulence of *P. sojae*.

Sequence analysis revealed that the nuclear protein PINP1 is evolutionarily conserved among eukaryotes (Qiao et al., 2015). To determine the association between PSR1 and other PINP1 orthologs, we first performed bimolecular fluorescence complementation (BiFC) assays. PSR1 and PINP1 orthologs were fused to either the N- or the C-terminal half of YFP (nYFP or cYFP, respectively) and transiently co-expressed in N. benthamiana. Intriguingly, a strong fluorescence signal was observed exclusively in the nucleus of N. benthamiana epidermal cells containing all combinations of PSR1 and PINP1 constructs (Supplemental Figure 2A). We then examined the association of these PINP1 orthologs with PSR1 in planta. N. benthamiana leaves were coinfiltrated with FLAG-PSR1 and each of nine YFP-HA-tagged PINP1 orthologs. Total proteins were extracted from the agroinfiltrated leaves and incubated with anti-GFP resin. Consistent with the BiFC assay results, all PINP1 orthologs, but not YFP-HA, were significantly enriched in the FLAG-PSR1 precipitate of plant cells (Supplemental Figure 2B). Because PINP1 encodes a DEAH-box pre-mRNA-splicing factor 16 (PRP16) (Wang et al., 1998), we examined the interaction between PSR1 and other PRPs. This experiment was performed by cloning the human (Homo sapiens) HsPRP5 and A. thaliana AtPRP5 and AtPRP22 genes, followed by Y2H and BiFC assays. Similar to the negative control, PSR1 was unable to bind to the three PRP factors (Supplemental Figure 3A, 3B). Together, these results indicate that PSR1 specifically associates with all PINP1 orthologs examined, but not with other types of splicing factors.

The DEAH, HA2, and DUF1605 domains of PINP1 are essential for its interaction with PSR1

To obtain insight into the interaction of PSR1 with PINP1, we mapped the PSR1-binding domain within PINP1. We generated a series of truncated PINP1 variants lacking different domains, and performed Y2H assays (Figure 1D). Our results showed that the six truncated PINP1 proteins (T1–T6) did not interact with PSR1, whereas the T7 variant of PINP1 lacking the N-terminal 558 amino acids (1–558) interacted with PSR1. This suggests that the C-terminus of PINP1 (559-1255) mediates interaction with PSR1 (Figure 1D). To narrow down the domain(s) of PINP1 required for binding to PSR1, we created seven *PINP1* deletion variants lacking either one, two, or three domains (D1-D7). Deletion of the PINP1 helicase C-terminal (Helicase C) domain compromised its binding to PSR1, unlike the individual deletions of the other three domains

(DEAH-like helicase [DEAH], Helicase-associated domain 2 [HA2], and domain of unknown function 1605 [DUF1605]), which did not compromise binding to PSR1 (Figure 1D). Further deletion analyses showed that the simultaneous loss of two or three domains of PINP1 completely abolished its interaction with PSR1, demonstrating that three domains of PINP1, including the DEAH, HA2, and DUF1605, are responsible for the interaction of PINP1 with PSR1.

To confirm the function of PSR1-binding domains *in planta*, we chose one deletion mutant (PINP1^{D1}), two truncation mutants (PINP1^{T2} and PINP1^{T7}), and full-length PINP1, and performed co-immunoprecipitation (Co-IP) assays in *N. benthamiana* leaves. Consistent with the results of Y2H assays, PINP1 and PINP1^{T7}, but not PINP1^{T2} and PINP1^{D1}, were significantly enriched in the PINP1-YFP precipitates from plant cells (Supplemental Figure 3C). Intriguingly, we observed that all deletion and truncation derivates of PINP1 (PINP1^{D1}, PINP1^{T2}, and PINP1^{T7}) localized to the nucleus of *N. benthamiana* leaf epidermal cells, similar to full-length PINP1 (Supplemental Figure 3D). Overall, these data suggest that the DEAH, HA2, and DUF1605 domains of PINP1 are required for its interaction with PSR1.

To better understand the role of key residues in the enzymatic domains of PINP1, we performed Ala-scanning mutagenesis and tested the effect of mutations in the active site of PINP1. We created ten mutated PINP1s (M1–M10) harboring substitutions in the DEAH and helicase domains, which are responsible for ATP binding and hydrolysis, RNA helicase, and RNA binding (Supplemental Figure 4A). Y2H assays showed that all mutated PINP1s interacted with PSR1 (Supplemental Figure 4B), indicating that the core catalytic site of PINP1 is unessential for binding to PSR1.

Functional complementation of the *prp16* deletion mutant yeast strain by *Arabidopsis PINP1*

To determine whether *PINP1* is a functional homolog of yeast *PRP16*, we tested the ability of *PINP1* to complement the yeast deletion strain $prp16\Delta$ BY4741 (here we named $prp16\Delta$ as $pinp1\Delta$), which exhibits a temperature-sensitive growth defect (Hotz and Schwer, 1998). The expression of *PINP1* in $pinp1\Delta$ restored the growth of yeast on synthetic complete medium when incubated at 37°C for 72 h, whereas transformation of $pinp1\Delta$ yeast cells with the empty vector

(EV) control failed to rescue growth (Figure 2), indicating that PINP1 functionally complements yeast PRP16. In addition, we found that the expression of $PINP1^{M2}$ (harboring a mutation in the RNA-binding site) and $PINP1^{M3}$ (harboring a mutation in the DEAHER motif) in $pinp1\Delta$ partially restored yeast growth. However, mutations in the active site residues of PINP1 completely abolished its ability to complement yeast PRP16 (Figure 2). Importantly, the data showed that $pinp1\Delta$ yeast cells transformed with PSR1-PINP1 (in which PSR1 and PINP1 were driven by two different promoters) could not grow on the synthetic complete medium (Figure 2), suggesting that PSR1 interferes with PINP1 functions in yeast. We confirmed the expression of these PINP1 mutants and PSR1 in $pinp1\Delta$ yeast strains by RT-PCR (Supplemental Figure 5), and ruled out the possibility that expression of PSR1 influenced yeast growth by potentially interacting with yeast PRP16. Although transformants expressing PSR1 slightly inhibited growth, they were able to grow on the synthetic complete medium at 37°C. Collectively, our results indicate that PSR1 specifically hinders PINP1, but not PRP16 functions in yeast.

PSR1 reduces the RNA-binding and helicase activities of PINP1

PINP1 belongs to the DEAH-box subfamily of RNA helicases, and was predicted to contain conserved ATPase and RNA-binding motifs. To examine the biochemical functions of PINP1, we cloned the full-length coding sequence (CDS) of *PINP1*, and expressed the resultant construct in *Escherichia coli* (Supplemental Figure 4C). We first determined the unwinding activity of PINP1 using partial RNA duplexes in a strand displacement assay, as described previously (Salman-Dilgimen et al., 2013). The double-stranded RNA (dsRNA) was stable, and no unwinding was observed in the absence of PINP1 or ATP. Efficient unwinding was detected in the presence of both PINP1 and ATP, and the unwinding rate increased with increase in the amount of ATP (Figure 3A). Interestingly, PINP1 also utilized CTP, UTP, and GTP as energy sources to unwind dsRNA in helicase reactions, but the amount of CTP, UTP, and GTP required for unwinding dsRNA was greater than that of ATP (Figure 3B), which has been reported previously for other DEAH-box helicases (Claude et al., 1991; Erkizan et al., 2015). More importantly, the data showed that unwinding activities of PINP1 were markedly reduced in the presence of PSR1 (Figure 3C), indicating that PSR1 impeded PINP1 activity.

Because helicases usually hydrolyze ATP to provide energy for unwinding DNA or RNA duplexes (Pyle, 2008), we investigated the ATPase activity of PINP1 by performing a colorimetric assay using malachite green reagent, which detects the free inorganic phosphate released in the ATP hydrolysis reaction. Compared with the standard phosphate solution, in the presence of RNA substrate, WT PINP1 showed higher ATP hydrolase activity than its mutated derivates. However, in the absence of RNA substrate, neither the WT PINP1 nor its mutant variants displayed ATPase activity (Figure 3D). Thus, similar to other DExH family helicases, PINP1 possesses an intrinsic ATPase activity as an energy source for DNA and RNA duplex unwinding (Salman-Dilgimen et al., 2013; Cordin et al., 2014).

We then assessed the RNA-binding activity of PINP1 by performing electrophoretic mobility shift assays (EMSAs) using biotin-labeled RNAs. PINP1 was unable to bind to 20-nt single-stranded RNA (ssRNA) and dsRNA (Figure 3E). We further explored whether the length of the RNA substrate affected the binding activity of PINP1. Results showed that PINP1 could bind to 80-nt ssRNA and dsRNA (Figure 3F); however, addition of PSR1 decreased this binding (Figure 3G). These results suggest that PSR1 impedes the RNA-binding activity of PINP1, similar to a cold probe (inhibitor).

PSR1 blocks the pri-mRNA-binding ability of PINP1

PSR1 and PINP1 did not interact with the sRNA regulatory pathway components in the Y2H and BiFC assays (Supplemental Figure 6). Additionally, PINP1 showed binding to long ssRNA and dsRNA (Figure 3F). Therefore, we examined whether PINP1 can bind to pri- or pre-miRNAs by performing EMSA assays. The *GST-HIS* and *PINP1-HIS* constructs were expressed in *E. coli* and purified using Ni-NTA agarose resin. The EMSA of recombinant proteins incubated with biotin-labeled pri-miR172a showed that PINP1-HIS, but not GST-HIS, was able to retain pri-miR172a, and the addition of unlabeled GST-PSR1 was able to wash off the biotin signal (Figure 4A), indicating that PSR1 blocked the PINP-pri-miR172a binding. However, PINP1-HIS was unable to retain pre-miR172a in the EMSA. Similar results was obtained for the PINP1-pri-miR159b binding (Figure 4A), suggesting that PSR1 hinders the activity of PINP in pri-miRNA processing.

Next, we determined whether PINP1 binds pri-miRNA *in vivo*. RNA immunoprecipitation assay (RIP) was performed on the seedlings of two PINP1-overexpressing lines harboring the 35S_{pro}:PINP1-YFP-HA transgene (PINP1-YFP-HA-29 and PINP1-YFP-HA-44) (Ren et al., 2012; Qiao et al., 2015). After cross-linking, nuclear isolation, and IP, the presence of pri-miRNA in the PINP1 complex was examined with RT-PCR. All the pri-miRNAs tested were enriched in the PINP1-YFP-HA immunoprecipitates, but not in the YFP-FLAG complex from transgenic plants (Figure 4B). In addition, the control UBIQUITIN 5 (UBQ5) mRNA was not detected in the PINP1 complex (Figure 4B). To confirm the effect of PSR1 on the association between PINP1 and pri-miRNAs, we transiently overexpressed the PINP1, pri-miRNAs, with and without PSR1 in *N. benthamiana* leaves, and then analyzed the samples by RIP. Results showed that PSR1 consistently reduced the ability of PINP1 to bind to the pri-miRNA172a and pri-miRNA159b that were used in *in vitro* processing assays (Figure 4C). Together, these results show that PSR1 significantly impairs the pri-mRNA-binding ability of PINP1 *in vitro* and *in vivo*.

PSR1 overexpression and PINP1 silencing result in genome-wide IR

To assess the role of PINP1 as a core functional splicing factor, we performed RNA-seq and examined genome-wide changes in AS and gene expression in Col-0 (WT), *PINP1*-silenced line PINP1i-7, and *PSR* overexpression line PSR1-22. A total of 638,167,155 paired-end reads were generated, and more than 95.6% of the reads were perfectly aligned to the TAIR10 reference genome (Supplemental Figure 7). Quality control of the RNA-seq data confirmed its robustness and reproducibility and ensured the reliability of subsequent analyses (Supplemental Figure 8A, 8B). Intriguingly, comparison of mapping frequency among samples revealed that reads mapped to intronic regions were significantly higher in PINP1i-7 and PSR1-22 than in Col-0, but the three genotypes showed no differences in the number of reads mapped to 3' untranslated region (3'UTR), 5'UTR, and CDS (Supplemental Figure 8C). These data indicate that AS events occur at the posttranscriptional level in PINP1i-7 and PSR1-22 because of abnormal pre-mRNA splicing.

To identify abnormal splicing events regulated by PSR1 and PINP1, we investigated changes in AS in PINP1i-7 and PSR1-22. A total of 8,305 and 12,057 AS events, corresponding to 6,159 and 8,370 genes, respectively, were identified in the PINP1i-7 and PSR1-22 plants compared

with the WT (control), respectively (Figure 5A and 5B, Supplemental Data Set 1). Among the different AS events, IR events were the most predominant (93.8%, 95.6%), followed by A3SS (3.3%, 2.3%), A5SS (1.8, 1.5%), ES (0.9%, 0.6%), and MXE (0.1%, 0.1%) events in PINP1i-7 and PSR1-22 plants, respectively. Importantly, many significant overlapping events and/or genes in IR (64.3% [PINP1i-7] and 88.8% [PSR1-22]), A3SS (43.9% and 45.7%), A5SS (54.5% and 49.3%), and ES (54.5% and 57.1%) were identified between the two genotypes. These common AS events modified the transcripts of 5,295 genes. Most of the AS events in introns occurred in the same direction and at the same position, and the values were highly consistent (Figure 5B, Supplemental Figure 9). Given that PINP1 acts as a PSR1-interacting protein in plants, it is possible that PSR1 regulates AS by binding to and suppressing the splicing function of PINP1.

Genes exhibiting AS in PSR1-22 and PINP1i-7 are closely related to gene silencing and defense response pathways

To further examine the functions of genes encoding transcripts with common five AS events, we further analyzed same changes 5,135 bearing AS genes simultaneously identified in PINP1i-7 and PSR1-22 plants (Supplemental Data Set 2). Heatmap and gene expression (fold-change) correlation analyses showed that transcriptome data were highly concordant in IR, and gene expression patterns in both PINP1i-7 and PSR1-22 were similar to those in Col-0 (mock) (Figure 5C, Supplemental Data Set 3). Gene ontology (GO) enrichment analysis showed that the corresponding genes were enriched in GO terms such as 'hormone signal', 'spliceosome', 'RNA degradation', and 'RNA transport and surveillance' (Figure 5D). Intriguingly, we found that many silencing and defense response related genes contained IR events (Supplemental Data Set 3). Given that IR was the most predominant AS event in this study, we focused on investigating the biological functions of IR events.

To identify differential AS events, we randomly selected 21 IR, two SE, one A5SS, and three A3SS events according to the RNA-seq data, and confirmed the transcript levels of different isoforms by real-time PCR (RT-PCR) and quantified signal intensities of nine events. The 21 AS events included sRNA biogenesis factors, jasmonic acid (JA) related genes, and RNA splicing genes (Figure 6A, 6B, Supplemental Figures 10 and 11). For most IR events, and A5SS and A3SS cases, the signal intensity of intron-retaining isoforms (upper bands) of most of the transcripts

were enhanced in PSR1-22 and PINP1i-7 plants relative to that in Col-0 (wild type) plants, whereas, those of intron-spliced isoforms (lower bands) were relatively reduced. The ratio of intron-spliced to intron-retaining transcripts was obviously altered. For SE, the signal intensity of both intron-retained and intron-spliced isoforms of RS40 transcripts were increased in PSR1-22 and PINP1i-7 plants relative to that of wild type (Figure 6B). Interestingly, we found that many microRNA (miRNA) target genes undergo IR alteration (Supplemental Figure 12). RT-PCR analysis further revealed that IR occurred in the 14th exon of *DCL1*, leading to the production of truncated proteins lacking their PAZ, RNaseIII, and dsRBD domains, although this result was detected with the RNA-seq data (Supplemental Figure 13). In addition, qRT-PCR analysis revealed that transcript levels of five genes that exhibited IR (*DCL3*, *NRPD1*, *SE*, *AGO4* and *AOC2*) were upregulated in PINP1i-7 and PSR1-22 plants. This result was also confirmed by analyzing seven other sRNA- and salicylic acid (SA)-related genes, which generated intron-retaining isoforms (Figure 6C). Taken together, these results suggest that overexpression of *PSR1* or silencing of *PINP1* can modify IR occurrence and expression of many crucial sRNA-related, pathogenesis related (PR), and other regulatory genes in *Arabidopsis*.

Genes with increased IR enhance pathogen infection in N. benthamiana

Recently, an intron retention variant of PtRD26 from *Populus tomentosa* produced a truncated protein PtRD26^{IR}, which functions as a negative regulator of senescence by regulating multiple NAC transcription factors in *Populus* (Wang et al., 2021). This result prompted us to test whether the intron-retaining transcripts in PINP1i-7 and PSR1-22 plants were translated into proteins. To this end, we chose two genes with intron-retaining isoforms (*DCL2* and *DCL3*) and performed immunoblotting to examine protein expression using a gene-specific antibody. Both the intronspliced and intron-retaining isoforms in *DCL2* encoded the predicted proteins (DCL2 and DCL2^{IR}) in all plants tested. However, expression of the truncated DCL2^{IR} proteins generated by the mis-spliced RNAs was dramatically stronger in PINP1i-7 and PSR1-22 plants than that in wild type. By contrast, the full-length DCL2 proteins produced by correctly spliced mRNA did not clearly change in these plants (Figure 7A, upper panel). The truncated DCL3^{IR} proteins generated by the mis-spliced RNAs were only detected in PINP1i-7 and PSR1-22 plants, but not in Col-0 plants, and expression of the full-length DCL3 protein produced by the correctly spliced

mRNA was weaker in PINP1i-7 and PSR1-22 plants than that in Col-0 plants (Figure 7A, Lower panel). These results indicate that the intron-retaining isoforms are translated into putative truncated proteins in PINP1i-7 and PSR1-22 plants.

To determine the role of these IR-generated, putative truncated proteins in plant defense, five sRNA and JA signaling pathway related genes (AGO4, CPL4, AOC2, OPCL1, and MES10) were transiently expressed in *N. benthamiana* leaves, and pathogen inoculation assays were performed. AOC2 regulates the production of 12-oxo-phytodienoic acid (OPDA), a precursor of JA, and the AOC2.1 transcript generates a functional allene oxide cyclase, whereas the AOC2.2 is an IR transcript, which results in the production of a truncated protein lacking the AOC enzymatic domain (Supplemental Figure 13C). Functional analysis showed that overexpression of AOC2.1 in N. benthamiana reduced Phytophthora parasitica invasion compared with the GFP control, whereas overexpression of AOC2.2 had no significant effect on P. parasitica growth (Figure 7B, Supplemental Figure 14), indicating that the AOC2 functional isoform is a positive regulator of plant defense against P. parasitica infection. RNA-seq data and qRT-PCR results also showed that the transcript level of AOC2 was higher in both PINP1i-7 and PSR1-22 compared with the WT (Figure 6C), implying that the alteration of the unspliced isoform involved in pathogen resistance, AOC2.1, is suppressed by AOC2.2. Similar results were obtained when the AGO4, CPL4, OPCL1, MES10, and their corresponding intron-retaining transcripts were transiently expressed in N. benthamiana leaves (Figure 7B, Supplemental Figure 14). Furthermore, Compared to empty vector, AOC2- and CPL4-silenced N. benthamiana leaves were more susceptible to *Phytophthora capsici* than the empty vector controls, as manifested by increased lesion size and biomass (Figure 7C–7G). In addition, we further examined the functions of AOC2 and AGO4 in plant defense by analyzing of loss-of-function mutants in Arabidopsis. Results revealed that the ago4 and aoc2 mutants were more susceptible to P. parasitica than wild-type plants (Figure 7H, 7I). These data suggest that the PSR1-PINP1 interaction regulates plant immunity by inhibiting the normal RNA splicing of some PR gene-related immune regulatory factors.

DISCUSSION

Emerging data demonstrate that alternative RNA splicing plays a pivotal role in plant–pathogen interactions (Rigo et al., 2019). IR is the most prevalent AS event in plants; however, the underlying biological functions causing IR in plants remain largely unexplored. In this study, we demonstrated that the functional pre-mRNA splicing factor PINP1/PRP16 is a repressor of innate immune and gene silencing transcripts, and we revealed the molecular mechanism of PSR1 regulation by PINP1 in plants. We propose that PSR1 regulates global IR events by binding to and suppressing the pre-mRNA splicing and RNA-binding activities of PINP1 (Figure 8), thus dampening the initial induction of innate immune gene expression and pri-miRNA processing.

PSR1 was previously shown to promote pathogen infection in *Arabidopsis*, *N. benthamiana*, and soybean (Qiao et al., 2013; Zhang et al., 2019). Consistent with previous studies, our data further confirmed that the CRISPR/Cas9-edited *PSR1* contributes to *P. sojae* virulence on susceptible host plants (Figure 1). Together, these results imply that PSR1 is a virulence factor that counteracts plant immunity to facilitate pathogen growth. In addition, our results demonstrated that PSR1 interacts with all orthologs of PINP1 in plants, animals, and oomycete that we tested (Supplemental Figure 2), suggesting that the pre-mRNA splicing function of PINP1 orthologs is conserved. Intriguingly, our data showed that PSR1 also binds to the *P. sojae* PsPINP1 protein. We propose that PsPINP1 possesses a special self-defense ability or substrate specificity. Because most oomycete genes have few or no introns, the function of PsPINP1in the spliceosome is probably normal and protected through an unknown mechanism (Shen et al., 2011; Judelson, 2012). However, the mode of action of PSR1 on the PsPINP1–spliceosome complex in *P. sojae* remains to be investigated.

Although yeast and human spliceosomes are well studied (Galej et al., 2016; Fica et al., 2017; Zhan et al., 2018), plant spliceosomes have not yet been isolated. Comparative genomic analyses revealed that the number of splicing regulatory factors in *Arabidopsis* is more than twice that in humans (Reddy et al., 2013), but their precise assembly, composition, and functions remain obscure. Arabidopsis *PINP1* is predicted to encode a pre-mRNA splicing factor PRP16 that triggers a key spliceosome conformational switch to facilitate the second step of splicing (Semlow et al., 2016; Vijayakumari et al., 2019). Concordant with homolog functions in yeast and human, our results showed that the silencing of *PINP1* affected genome-wide AS in plants.

Additionally, PINP1 could bind to 80-nt ssRNA and dsRNA (Figure 3). Intriguingly, PINP1 was also able to bind to pri-miRNAs *in vitro* and *in vivo*, but its binding ability was blocked by PSR1, indicating a link between the roles of PSR1 and PINP1 in sRNA biogenesis (Qiao et al., 2015; Tsugeki et al., 2015; Qiao et al., 2021). Nevertheless, some PINP1 homologs, such as those from *Chlamydomonas reinhardtii* and the nematode *Meloidogyne incognita*, do not play a central role in pre-mRNA splicing but mediate gene silencing and sex determination (Puoti and Kimble, 1999; Wu-Scharf et al., 2000). Our data showed that *Arabidopsis* PINP1 plays dual roles in RNA silencing and pre-mRNA splicing.

Although the splicing assay has been well established and applied in animal and human spliceosomes studies, the RNA splicing machinery of spliceosomes is not well characterized in plants (Rigo et al., 2019; Wilkinson et al., 2020). Recently, an *in vitro* splicing assay was developed using plant nuclear extracts (Albaqami and Reddy, 2018). In the present study, we demonstrated that PINP1 is an active RNA helicase, but we could not elucidate the relationship between its enzymatic activities and splicing ability. Future studies are needed to determine whether the RNA helicase activity of PINP1 is closely dependent on its pre-mRNA splicing ability.

RNA-seq of genome-wide AS events in animals and plants show that pathogen infection can affect the inclusion or exclusion of exons from mature mRNAs (Chaudhary et al., 2019; Rigo et al., 2019; Huang et al., 2020). This implies that pathogen infection-induced AS depends on the selective utilization of endogenous regulators, thereby suggesting possible crosstalk and cross-regulation between pathogenic factors and the host splicing machinery. Regulation of AS during viral infection has been well characterized. An exciting example is offered by the NS1 protein of the influenza A virus, which interacts with the spliceosome complex and blocks the spliceosome transition to the active complex by inhibiting cellular gene expression (De Maio et al., 2016). Unlike viral infections, much less is known about *Phytophthora* and bacterial virulence factors that interfere with the host RNA splicing machinery. HopU1, a type III effector from *Pseudomonas syringae*, targets the host GRP7 protein, which affects the AS of certain transcripts via direct interaction with their mRNAs (Streitner et al., 2012). More recently, the *P. sojae* effector PsAvr3c was shown to bind to and stabilize soybean GmSKRPs, which are associated

with plant spliceosome components that mediate AS events and subsequently negatively regulate plant immunity (Huang et al., 2017).

In the current study, PSR1 altered the host RNA splicing by specifically interacting with the core spliceosome component PINP1. Thus, the mechanism employed by PSR1 resembled those employed by the NS5 and NS1-BP proteins of the influenza A virus(De Maio et al., 2016; Thompson et al., 2018). Moreover, specific subsets of IR transcripts have been proposed to be regulated posttranscriptionally by sRNAs and the immune response. Indeed, we identified over 5,102 splicing events in 4,932 genes co-regulated by PINP1 and PSR1 (Figure 6), indicating widespread cooperation between these two proteins. Kyoto Encyclopedia of Genes and Genomes (KEGG) pathway enrichment analysis showed that 'protein processing', 'RNA degradation', 'spliceosome', 'RNA transport', and 'purine metabolism' pathways were significantly enriched classes of genes represented in PINP1 and PSR1, and many of the pre-mRNAs regulated by PINP1 and PSR1 encode proteins involved in sRNA biogenesis and plant immunity.

Our data indicated that IR events represent more than 80–90% of all AS events. Many sRNAand defense-related genes are associated with IR generation, and the expression of these genes is upregulated at the occurrence of IR. Recently, RNA NMD has been previously reported as an important virulence strategy for plant and animal viruses (Balistreri et al., 2014; Garcia et al., 2014). Transcripts with retained intron resulting from alteration in PINP1 function may be degraded by the nuclear RNA surveillance machinery or the cytoplasmic NMD pathway. Alternatively, these intron-retaining transcripts could be translated into new protein variants. Strikingly, our data indicate that the intron-retaining DCL2 and DCL3 isoforms were translated into truncated proteins. However, the fate of most of the intron-retaining transcripts identified in this study was not determined, Future studies will determine if these other intron-retaining transcripts are degraded or translated into truncated or new protein variants. Overall, this study provides comprehensive bioinformatic analyses of AS events and experimental validation of the significance of PSR1-PINP1 interaction in mediating plant immunity. We demonstrate that PSR1-PINP1 interaction blocks the PINP1-dependent functions, resulting an increase in PINP1mediated AS events. Furthermore, the data show that the decreased capability of PINP1 to bind RNA impedes the efficient processing of PINP1 target transcripts involved in sRNA biogenesis and plant immunity.

Materials and Methods

Plants, microbial strains and growth conditions

Arabidopsis thaliana Col-0 was used as the wild type (WT). All *Arabidopsis* lines and *N. benthamiana* plants were grown at 22°C, and soybean (*Glycine max*) was cultivated at 24°C in an environmentally controlled growth room under long photoperiod conditions (16 h/8 h light/dark). The relative humidity during the day and night was 50%. Light intensity was approximately 100–130 μmol photons m⁻² s⁻¹ PPFD. *Arabidopsis* for mRNA stability studies was grown aseptically on sterile Murashige and Skoog (MS) medium. *P. sojae* isolate P6497, *P. capsici* isolate PC35 and *P. parasitica* isolate PBS32 are regularly maintained on 10% V8 medium at 25°C in the dark. Primers used in this study are listed in Supplemental File 2.

P. sojae transformation and inoculation assay

Stable genetic transformation and putative transformant screening in *P. sojae* was performed using the CRISPR/Cas9 system as previously described (Fang and Tyler, 2016). Briefly, polyethylene glycol-mediated protoplast transformation approach was used to obtain transformants, and the putative transformants were propagated on V8 medium with 50 μ g mL⁻¹ G418 at 25°C.

The virulence of *P. sojae* transformants was determined by inoculation of etiolated soybean seedlings (*Glycine max* Chinese susceptible cv HuaChun6, HC6) and comparison of *P. sojae* biomass. Approximately 0.2 cm² mycelium plugs of each transformant and the wild-type strain were inoculated on 10-15 hypocotyls of 5 d-old etiolated soybean seedlings. The inoculated hypocotyls were maintained in the dark and high humidity at 25 °C. Virulence was evaluated using qPCR to quantify the ratios of *P. sojae* to soybean DNA in the inoculated tissue. Photographs were taken 48 hpi.

Yeast two-hybrid (Y2H) assay

Full-length coding sequences (CDSs) of PINP1 and PSR1 (without the signal peptide) were cloned into the bait vector pGBKT7 (Clontech, USA), full-length CDS of 25 small RNA-related factors, *PINP1*, nine *PINP1* homologs, 24 *PINP1* mutants, *HsPRP5*, *AtPRP5*, and *AtPRP22* were individually inserted into the prey vector pGADT7 (Clontech, USA). The AD-LaminC and AD-

SV40T were co-transformed with BD-p53 and served as negative and positive controls, respectively. The resultant bait and prey constructs across various combinations were co-transformed into the *S. cerevisiae* AH109 strain, the transformed cells were streaked on SD/–Trp/–Leu medium and incubated at 30°C for 2 d. Then, the cells were transferred on to the stringent medium (SD/–Trp/–Leu/–His/–Ade). Plates were incubated at 30°C for 4–8 d before evaluation and photography (Zhang et al., 2019).

BiFC and Co-IP assays

For BiFC assays, the full-length CDS of *PSR1* and 9 *PINP1* homologous genes were cloned into the pQBV3 vector, and subsequently recombined into the pEarleyGate201-YN and pEarleyGate202-YC vectors using Gateway LR Clonase. The resulting constructs were transformed into *Agrobacterium tumefaciens* strain GV3101, and then were transiently expressed in *N. benthamiana* leaves (Chen et al., 2020). The fluorescence signal (emission wavelength 512 nm) of interacting proteins was detected at 48 hpi using a confocal microscope (Olympus Fluoview FV1000).

For Co-IP assay, PCR amplification products were ligated into the pQBV3 and pQBV3-3×Flag vectors, and then recombined into the pEarleyGate100 and pEarleyGate101 vectors to produce various constructs, respectively. The YFP-HA plasmid was served as a negative control. The Flag-PSR1 was transiently co-expressed in *N. benthamiana* leaves, together with PINP1-YFP-HA, 9 YFP-HA tagged PINP1 homologous genes and three PINP1 mutants using *A. tumefaciens* strain GV3101-mediated infiltration, respectively. Total proteins were extracted using an extraction buffer [1 M Tris-HCl (pH 7.5), 5 M NaCl, 0.5 M EDTA, 20% glycerol, 10 mM DTT, 1× protease inhibitor (Sigma-Aldrich), 20% Triton X-100, and 2% PVPP], 1 mM PMSF, and 0.1% CA-630], and then incubated with anti-GFP magnetic beads (1:1,000 MBL, D153-11) at 4°C for four hours. Co-precipitation signal of PINP1 homologs or mutants were determined by immunoblotting using an anti-FLAG (1:5,000; MBL, M185-3L) or anti-HA antibody (1:5,000; MBL, M180-3).

Yeast transformation and complementation assay

Full-length or mutated CDS of PINP1 were cloned into the pESC vector, and the resultant plasmids were individually transformed into wild-type BY4741 and mutated Δ*PINP1/PRP16* yeast strains according to the manufacturer's protocol (Clontech, USA). The empty vector pESC was used as a negative control. The temperature sensitivity of cell growth ability for the resulting transformants were determined. Yeast cells were cultured on a synthetic medium (containing 2% galactose and lacking Leu) at 30°C and 37°C for 4-6 d before assessment and photography.

Recombinant protein production and purification

Full-length CDS of PINP1 and various PINP1 mutants were cloned directly into the pET-28a (Novagen, USA) expression vector. PCR product of PSR1 was inserted into the pGEX-4T-2 expression vector. These resulting recombinant plasmids and empty vector were individually transformed into competent cells of *E. coli* strain Rosetta DE3. The recombinant protein was induced by adding 0.1 mM IPTG (isopropyl β-D-1-thiogalactopyranoside) and incubated at 16°C overnight. PINP1-HIS and its mutated derivatives were purified using NiNTA-agarose resin (Qiagen) following the manufacturer's recommendations. Glutathione S-transferase (GST)-PSR1 was purified from crude lysates by affinity for immobilized glutathione-agarose (Sigma). The purified proteins were assessed by subjecting to 10% SDS-PAGE electrophoresis and Coomassie Brilliant Blue staining.

RNA duplex unwinding ATPase assays

The RNA substrate was prepared as previously described with slight modifications (Salman-Dilgimen et al., 2013). Briefly, an 84-nt DNA strand was amplified using linearized pET14b (Novagen, USA) plasmid as template, then subjected to *in vitro* transcription and removal of template DNA according to the manufacturer's instructions (MEGAshortscriptTM). The 37-nt short strand RNA was directly synthesized (Nanjing Jinsi Biotech) to be complementary to the middle region of the long strand RNA. For RNA unwinding assay, partial RNA duplex was generated by annealing an 84-nt RNA with a 37-nt long biotin-labeled RNA oligonucleotide (PierceTM RNA 3' End Biotinylation, Therom). The reaction mixtures (10 μL) contained 20 mM HEPES-KOH (pH 7.5), 2 mM MgCl₂, 2 mM ATP, 20 U ml⁻¹ RNasin, 0.25 pM RNA substrate,

and the purified protein. Reactions were incubated 50 min at 37°C, then separated on an 8% native polyacrylamide gel, detected using the Chemiluminescent Nucleic Acid Detection Module kit (Thermo) and visualized using an Amersham Imager 600 (GE Healthcare). For ATPase assay, ATPase measurements were performed in 1-mL reaction mixtures. Release of inorganic phosphate was determined continuously using PiPerTM Phosphate Assay Kit (Thermo).

RNA binding assay

Two 20-nt single-strand complementary RNAs were synthesized (Nanjing Jinsi Biotech). PremiRNAs and 84-nt single-strand complementary RNAs were synthesized as described above. Four substrate RNAs were labeled with biotin using the PierceTM RNA 3' End Biotinylation Kit (Thermo). The RNA-binding assay was performed as described (Ren et al., 2012; Qiao et al., 2013). Briefly, RNA-binding reaction mixtures (20 μL) containing 10 mM HEPES (PH 7.3), 20 mM KCl, 1 mM MgCl₂, 1 mM DTT, 20 U RNase inhibitor, 5 ug tRNA, 5% glycerol, 0.1 pmol biotin labeled RNA, and specific protein. The reaction was incubated for 30 min at room temperature, then separated on an 8% native polyacrylamide gel, detected using Chemiluminescent Nucleic Acid Detection Module kit (Thermo) and visualized by an Amersham Imager 600 (GE Healthcare).

RNA Immunoprecipitation (RIP)

RIP assays were performed as described previously (Ren et al., 2012; Ji et al., 2021). For transgenic *Arabidopsis* plants, about 2 g of young leaf tissue was crosslinked with 1% formaldehyde by vacuum infiltration for 40 min and quenched by adding Gly to a final concentration of 0.125 M for 10 min. The nuclear fractions were extracted, and then incubated with anti-GFP antibodies (1:100; MBL, D153-11) overnight at 4 °C. PINP1-associated RNAs were then extracted and analyzed with RT-PCR. For transient assays in *N. benthamiana*, *PINP1-YFP-HA* and six *MIR* genes with/without PSR1-3*FLAG were transiently co-expressed in *N. benthamiana* leaves. Approximately 3 g of leaves were used for RIP analysis.

RNA isolation, RT-PCR and qRT-PCR

Plant total RNA was extracted using the TRIZOL reagent (Invitrogen). Yeast total RNA was isolated using an RNA kit according to the manufacturer's instructions (Beijing Zhuangmeng International Bio-Gene Technology Co., Ltd.). A 1-µg aliquot of total RNA was reverse transcribed by priming with oligo (dT18) in a 20-µL reaction volume using the PrimeScript Reverse Transcriptase kit (Takara, Otsu, Japan). Soybean *CYP2* used as internal control. qRT-PCRs were performed using the gene-specific primers as previously described (Zhang et al., 2019, Supplemental File 2).

RNA sequencing (RNA-Seq) analysis and validation of AS events

RNA-Seq libraries were constructed according to the manufacturer's procedure. An Illumina HiSeqTM 2500 was used as a platform for RNA-Seq via Beijing Novogene Bioinformatics Technology Co. Ltd. Raw RNA-Seq reads were assessed for quality control by software Trimmomatic v0.32 (Bolger et al., 2014). Then, clean reads were aligned to the TAIR10 *Arabidopsis* genome by Hisat2 (Kim et al., 2019). The number of fragments per kilobase (FPKM) of transcripts per thousand fragments was calculated using the StringTie (Pertea et al., 2015) and analysis of differentially expressed genes was performed by DEseq2 (fold changes >2 and adjusted P value < 0.05). Five pre-mRNA splicing events containing exon skip (ES), alternative 5' splice sites (A5SS), alternative 3' splice sites (A3SS), and mutually exclusive exons (MXE), intron retention (IR) were identified and analyzed by rMATS v3.2.5 (Shen et al., 2014). A p-value less than 0.05 is considered a differential alternative splicing event. The validity of AS events was calculated by using isoform-specific primers (Supplemental File 2).

Subcellular localization

The full-length CDS was cloned into the expression vector pEarleyGate101. The recombinant plasmid was transformed into *A. tumefaciens* strain GV3101 and were expressed in 3-week-old *N. benthamiana* leaves, and their signals in plant cells were examined using a confocal microscope (Olympus Fluoview FV1000) at 48 hpi.

Phytophthora infection assay in N. benthamiana

Plasmids of gene and its IR isoforms were transiently expressed in *N. benthamiana* leaves via *A. tumefaciens*-mediated infiltration, respectively. After 24 h, the leaves were detached and inoculated with about 2,000 *P. parasitica* zoospores in suspension. Inoculated leaves were incubated in a growth chamber at 24°C for 2 to 3 d before analysis of disease progression. The *P. parasitica* lesions were measured and photographed under a UV lamp.

Leaf discs of *N. benthamiana* were sampled from infected site 40 to 60 h after *P. capsici* inoculation. Pure genomic DNA was extracted using a genomic DNA extraction kit (TIANGEN Biotech, Beijing, DP305-02). *P. capsici* biomass in inoculated leaves was determined by qPCR using primers specific for *N. benthamiana* and *P. capsici* actin genes (Supplemental File 2). Three independent biological replicates were performed.

Accession numbers

Sequence data from this article can be found in the GenBank (NCBI) / Arabidopsis TAIR database (www.arabidopsis.org) under the following accession numbers: PSR1 (XM 009519945.1), PINP1 (AT5G13010), MIR159b (AT1G18075), MIR172a (AT2G28056), MIR319a (AT4G23713), MIR393a (AT2G39885), MIR398a (AT2G03445), NRPD1 (AT1G63020), SE (AT2G27100), AOC2 (AT3G25770), RS40 (AT4G25500), CKB3 (AT3G60250), KAS (AT2G04540), OPCL1 (AT1G20510), MES10 (AT3G50440), MES3 (AT2G23610), IAR3 (AT1G51760), MORC6 (AT1G19100), CPL4 (AT5G58003), SKI3 (AT1G76630), ROS1 (AT2G36490), ROS3 (AT5G58130), HMGA (AT1G14900), RID1 (AT1G26370), NUA (AT1G79280), SKI2 (AT3G46960), TRN1 (AT2G16950), NOT2A (AT1G07705), ELF3 (AT2G25930), BGAL9 (AT2G32810), 4CL3 (AT1G65060), MYB65 (At3g11440), MYB33 (At5g06100), ARF17 (At1g77850), PHV (At1g30490), ATHB-15 (At1g52150), ARF8 (At5g37020), NF-YA8 (At1g17590), ATHAP2B (At3g05690), ATHAP2A (At5g12840), TOE1 (At2g28550), AP2 (At4g36920), TOE3 (At5g67180), AFB3 (At1g12820), AFB1 (At4g03190), GRF3 (At2g36400), ATK2 (At4g27180), StPINP1 (XM 015304082.1), CaPINP1 (XM 016688552.2), SIPINP1 (XM 004249042.4), HsPINP1 (NM 014003.4), DmPINP1 (NM 132719.3), MmPINP1 (NM 178380.2), PsPINP1 (PHYSODRAFT 115314), PiPINP1 (XM 002998888.1), PpPINP1 (XM 008915836.1), HsPRP5 (NM 001300860.2),

AtPRP5 (At3g26560), AtPRP22 (At1g26370), AGO1 (AT1G48410), AGO2 (AT1G31280), AGO3 (AT1G31290), AGO4 (AT2G27040), AGO5 (AT2G27880), AGO6 (AT2G32940), AGO7 (AT1G69440), AGO8 (AT5G21030), AGO9 (AT5G21150), AGO10 (AT5G43810), DCL1 (AT1G01040), DCL2 (AT3G03300), DCL3 (AT3G43920), DCL4 (AT5G20320), HEN1 (AT4G20910), HASTY (AT3G05040), CPL1 (AT4G21670), CPL2 (AT5G01270), RCF3 (AT5G53060), CBP20 (AT5G44200), CBP80 (AT2G13540), DDL (AT3G20550), HYL1 (AT1G09700), STA1 (AT4G03430), NbAOC2 (Niben101Scf13816g00005.1), NbCPL4 (Niben101Scf00209g00009.1), UBQ5 (AT3G62250), Actin1 (AT2G37620), GmCYP2 (Glyma.12g024700), ScALG9 (NM 001183057.1).

Data availability

RNA-seq data generated in this study have been deposited in Gene Expression Omnibus (GEO) database (https://www.ncbi.nlm.nih.gov/geo/query/acc.cgi?acc=GSE188606) under the accession codes GSE188606.

Supplemental data

The following materials are available in the online version of this article.

Supplemental Figure 1. Knockout of the PSR1 effector in *P. sojae* by using the CRISPR/Cas9 system.

Supplemental Figure 2. PSR1 associates with PINP1 orthologs of plants, animals, and oomycetes.

Supplemental Figure 3. Analysis of interactions between PSR1 and three pre-mRNA splicing factors.

Supplemental Figure 4. Mutations in the catalytic core of PINP1 did not affect its interaction with PSR1 in Y2H assays.

Supplemental Figure 5. RT-PCR analyses of mRNA expression levels in $pinp1\Delta$ yeast strains for PSR1, PINP1, and various PINP1 mutants.

Supplemental Figure 6. PSR1 and PINP1 did not interact with small RNA regulatory pathway components in Y2H and BiFC assays.

Supplemental Figure 7. Summary information for mapping of RNA-seq reads to the *Arabidopsis* reference genome.

Supplemental Figure 8. Summary of RNA-seq data in nine samples.

Supplemental Figure 9. Venn diagrams summarizing overlapping splicing events.

Supplemental Figure 10. Validation of alternative splicing predictions by RNA-seq and RT-PCR.

Supplemental Figure 11. Validation of alternative splicing predictions by RT-PCR.

Supplemental Figure 12. Validation of intron retention events in miRNA target genes.

Supplemental Figure 13. Intron retention results in different protein isoforms.

Supplemental Figure 14. Function of the intron-retaining genes in plant defense.

Supplemental Data Set 1. Differential alternative splicing events in two transgenic Arabidopsis lines.

Supplemental Data Set 2. Gene expression of 5,135 common alternative splicing events in two transgenic Arabidopsis lines.

Supplemental Data Set 3. Differential expression of 5,104 common intron retention events in two transgenic Arabidopsis lines.

Supplemental File 1. Statistical analysis tables.

Supplemental File 2. Primers used in this study.

ACKNOWLEDGMENTS

We thank Prof. Weiman Xing (Shanghai Normal University) for suggestions in protein expression and purification. This work was supported by grants from the National Natural Science Foundation of China (32072502, 32172359, and 31522045), the "Shuguang Program" of Shanghai Education Development Foundation and Shanghai Municipal Education Commission, and the Science and Technology Commission of Shanghai Municipality (18DZ2260500).

AUTHOR CONTRIBUTIONS

YQ conceived and designed the experiments; XG, PZ, DW, ZD, XW, and JS performed the experiment; PZ and ZD analyzed the data; QS, YZX, and WM provided the suggestion for this

research; YQ and XG wrote the manuscript. All authors discussed the results and commented on the manuscript.

COMPETING INTERESTS

The authors declare no competing interests.

REFERENCES

- **Albaqami, M., and Reddy, A.S.N.** (2018). Development of an in vitro pre-mRNA splicing assay using plant nuclear extract. Plant Methods **14,** 1.
- Balistreri, G., Horvath, P., Schweingruber, C., Zund, D., McInerney, G., Merits, A., Muhlemann, O., Azzalin, C., and Helenius, A. (2014). The host nonsense-mediated mRNA decay pathway restricts Mammalian RNA virus replication. Cell Host Microbe 16, 403-411.
- **Bolger, A.M., Lohse, M., and Usadel, B.** (2014). Trimmomatic: a flexible trimmer for Illumina sequence data. Bioinformatics **30,** 2114-2120.
- Chaudhary, S., Khokhar, W., Jabre, I., Reddy, A.S.N., Byrne, L.J., Wilson, C.M., and Syed, N.H. (2019). Alternative Splicing and Protein Diversity: Plants Versus Animals. Front Plant Sci 10, 708.
- Chen, C., He, B., Liu, X., Ma, X., Liu, Y., Yao, H.Y., Zhang, P., Yin, J., Wei, X., Koh, H.J., Yang, C., Xue, H.W., Fang, Z., and Qiao, Y. (2020). Pyrophosphate-fructose 6-phosphate 1-phosphotransferase (PFP1) regulates starch biosynthesis and seed development via heterotetramer formation in rice (Oryza sativa L.). Plant Biotechnol J 18, 83-95.
- Claude, A., Arenas, J., and Hurwitz, J. (1991). The isolation and characterization of an RNA helicase from nuclear extracts of HeLa cells. J Biol Chem 266, 10358-10367.
- Cordin, O., Hahn, D., Alexander, R., Gautam, A., Saveanu, C., Barrass, J.D., and Beggs, J.D. (2014). Brr2p carboxy-terminal Sec63 domain modulates Prp16 splicing RNA helicase. Nucleic Acids Res 42, 13897-13910.
- **De Bortoli, F., Espinosa, S., and Zhao, R.** (2021). DEAH-Box RNA Helicases in Pre-mRNA Splicing. Trends Biochem Sci **46,** 225-238.

- De Maio, F.A., Risso, G., Iglesias, N.G., Shah, P., Pozzi, B., Gebhard, L.G., Mammi, P., Mancini, E., Yanovsky, M.J., Andino, R., Krogan, N., Srebrow, A., and Gamarnik, A.V. (2016). The Dengue Virus NS5 Protein Intrudes in the Cellular Spliceosome and Modulates Splicing. PLoS Pathog 12, e1005841.
- Erkizan, H.V., Schneider, J.A., Sajwan, K., Graham, G.T., Griffin, B., Chasovskikh, S., Youbi, S.E., Kallarakal, A., Chruszcz, M., Padmanabhan, R., Casey, J.L., Uren, A., and Toretsky, J.A. (2015). RNA helicase A activity is inhibited by oncogenic transcription factor EWS-FLI1. Nucleic Acids Res 43, 1069-1080.
- **Fang, Y., and Tyler, B.M.** (2016). Efficient disruption and replacement of an effector gene in the oomycete Phytophthora sojae using CRISPR/Cas9. Mol Plant Pathol **17,** 127-139.
- Fica, S.M., Oubridge, C., Galej, W.P., Wilkinson, M.E., Bai, X.C., Newman, A.J., and Nagai, K. (2017). Structure of a spliceosome remodelled for exon ligation. Nature **542**, 377-380.
- Galej, W.P., Wilkinson, M.E., Fica, S.M., Oubridge, C., Newman, A.J., and Nagai, K. (2016). Cryo-EM structure of the spliceosome immediately after branching. Nature **537**, 197-201.
- **Garcia**, **D.**, **Garcia**, **S.**, **and Voinnet**, **O.** (2014). Nonsense-mediated decay serves as a general viral restriction mechanism in plants. Cell Host Microbe **16**, 391-402.
- Garcia, D., Garcia, S., Pontier, D., Marchais, A., Renou, J.P., Lagrange, T., and Voinnet, O. (2012). Ago hook and RNA helicase motifs underpin dual roles for SDE3 in antiviral defense and silencing of nonconserved intergenic regions. Mol Cell 48, 109-120.
- **Hotz, H.R., and Schwer, B.** (1998). Mutational analysis of the yeast DEAH-box splicing factor Prp16. Genetics **149,** 807-815.
- Huang, J., Lu, X., Wu, H., Xie, Y., Peng, Q., Gu, L., Wu, J., Wang, Y., Reddy, A.S.N., and Dong, S. (2020). Phytophthora Effectors Modulate Genome-wide Alternative Splicing of Host mRNAs to Reprogram Plant Immunity. Mol Plant 13, 1470-1484.
- Huang, J., Gu, L., Zhang, Y., Yan, T., Kong, G., Kong, L., Guo, B., Qiu, M., Wang, Y., Jing, M., Xing, W., Ye, W., Wu, Z., Zhang, Z., Zheng, X., Gijzen, M., Wang, Y., and Dong, S. (2017). An oomycete plant pathogen reprograms host pre-mRNA splicing to subvert immunity. Nat Commun 8, 2051.
- Ji, H.M., Mao, H.Y., Li, S.J., Feng, T., Zhang, Z.Y., Cheng, L., Luo, S.J., Borkovich, K.A., and Ouyang, S.Q. (2021). Fol-milR1, a pathogenicity factor of Fusarium oxysporum,

- confers tomato wilt disease resistance by impairing host immune responses. New Phytol **232,** 705-718.
- **Judelson, H.S.** (2012). Dynamics and innovations within oomycete genomes: insights into biology, pathology, and evolution. Eukaryot Cell **11**, 1304-1312.
- Kim, D., Paggi, J.M., Park, C., Bennett, C., and Salzberg, S.L. (2019). Graph-based genome alignment and genotyping with HISAT2 and HISAT-genotype. Nat Biotechnol 37, 907-915.
- **Linder, P., and Owttrim, G.W.** (2009). Plant RNA helicases: linking aberrant and silencing RNA. Trends Plant Sci **14,** 344-352.
- Ma, Z., Zhu, L., Song, T., Wang, Y., Zhang, Q., Xia, Y., Qiu, M., Lin, Y., Li, H., Kong, L., Fang, Y., Ye, W., Wang, Y., Dong, S., Zheng, X., Tyler, B.M., and Wang, Y. (2017). A paralogous decoy protects Phytophthora sojae apoplastic effector PsXEG1 from a host inhibitor. Science 355, 710-714.
- Marquez, Y., Brown, J.W., Simpson, C., Barta, A., and Kalyna, M. (2012). Transcriptome survey reveals increased complexity of the alternative splicing landscape in Arabidopsis. Genome Res 22, 1184-1195.
- Moy, R.H., Cole, B.S., Yasunaga, A., Gold, B., Shankarling, G., Varble, A., Molleston, J.M., tenOever, B.R., Lynch, K.W., and Cherry, S. (2014). Stem-loop recognition by DDX17 facilitates miRNA processing and antiviral defense. Cell 158, 764-777.
- Nasif, S., Contu, L., and Muhlemann, O. (2018). Beyond quality control: The role of nonsense-mediated mRNA decay (NMD) in regulating gene expression. Semin Cell Dev Biol 75, 78-87.
- Pan, Q., Shai, O., Lee, L.J., Frey, B.J., and Blencowe, B.J. (2008). Deep surveying of alternative splicing complexity in the human transcriptome by high-throughput sequencing. Nat Genet 40, 1413-1415.
- Pertea, M., Pertea, G.M., Antonescu, C.M., Chang, T.C., Mendell, J.T., and Salzberg, S.L. (2015). StringTie enables improved reconstruction of a transcriptome from RNA-seq reads. Nat Biotechnol 33, 290-295.
- **Puoti, A., and Kimble, J.** (1999). The Caenorhabditis elegans sex determination gene mog-1 encodes a member of the DEAH-Box protein family. Mol Cell Biol **19,** 2189-2197.

- **Pyle, A.M.** (2008). Translocation and unwinding mechanisms of RNA and DNA helicases. Annu Rev Biophys **37**, 317-336.
- Qiao, Y., Shi, J., Zhai, Y., Hou, Y., and Ma, W. (2015). Phytophthora effector targets a novel component of small RNA pathway in plants to promote infection. P Natl Acad Sci USA 112, 5850-5855.
- Qiao, Y., Xia, R., Zhai, J., Hou, Y., Feng, L., Zhai, Y., and Ma, W. (2021). Small RNAs in Plant Immunity and Virulence of Filamentous Pathogens. Annu Rev Phytopathol **59**, 265-288.
- Qiao, Y., Liu, L., Xiong, Q., Flores, C., Wong, J., Shi, J., Wang, X., Liu, X., Xiang, Q., Jiang, S., Zhang, F., Wang, Y., Judelson, H.S., Chen, X., and Ma, W. (2013). Oomycete pathogens encode RNA silencing suppressors. Nat Genet 45, 330-333.
- **Reddy, A.S., Marquez, Y., Kalyna, M., and Barta, A.** (2013). Complexity of the alternative splicing landscape in plants. Plant Cell **25,** 3657-3683.
- Ren, G., Xie, M., Dou, Y., Zhang, S., Zhang, C., and Yu, B. (2012). Regulation of miRNA abundance by RNA binding protein TOUGH in Arabidopsis. Proc Natl Acad Sci U S A 109, 12817-12821.
- **Rigo, R., Bazin, J.R.M., Crespi, M., and Charon, C.L.** (2019). Alternative Splicing in the Regulation of Plant-Microbe Interactions. Plant Cell Physiol **60**, 1906-1916.
- Salman-Dilgimen, A., Hardy, P.O., Radolf, J.D., Caimano, M.J., and Chaconas, G. (2013). HrpA, an RNA helicase involved in RNA processing, is required for mouse infectivity and tick transmission of the Lyme disease spirochete. PLoS Pathog 9, e1003841.
- Scotti, M.M., and Swanson, M.S. (2016). RNA mis-splicing in disease. Nat Rev Genet 17, 19-32.
- Semlow, D.R., Blanco, M.R., Walter, N.G., and Staley, J.P. (2016). Spliceosomal DEAH-Box ATPases Remodel Pre-mRNA to Activate Alternative Splice Sites. Cell **164**, 985-998.
- **Shen, D., Ye, W., Dong, S., Wang, Y., and Dou, D.** (2011). Characterization of intronic structures and alternative splicing in Phytophthora sojae by comparative analysis of expressed sequence tags and genomic sequences. Can J Microbiol **57,** 84-90.

- Shen, S., Park, J.W., Lu, Z.X., Lin, L., Henry, M.D., Wu, Y.N., Zhou, Q., and Xing, Y. (2014). rMATS: robust and flexible detection of differential alternative splicing from replicate RNA-Seq data. Proc Natl Acad Sci U S A 111, E5593-5601.
- Shi, J., Jia, Y., Fang, D., He, S., Zhang, P., Guo, Y., and Qiao, Y. (2020). Screening and Identification of RNA Silencing Suppressors from Secreted Effectors of Plant Pathogens.

 J Vis Exp 156, e60697.
- Streitner, C., Koster, T., Simpson, C.G., Shaw, P., Danisman, S., Brown, J.W., and Staiger, D. (2012). An hnRNP-like RNA-binding protein affects alternative splicing by in vivo interaction with transcripts in Arabidopsis thaliana. Nucleic Acids Res 40, 11240-11255.
- Thompson, M.G., Munoz-Moreno, R., Bhat, P., Roytenberg, R., Lindberg, J., Gazzara, M.R., Mallory, M.J., Zhang, K., Garcia-Sastre, A., Fontoura, B.M.A., and Lynch, K.W. (2018). Co-regulatory activity of hnRNP K and NS1-BP in influenza and human mRNA splicing. Nat Commun 9, 2407.
- Tsugeki, R., Tanaka-Sato, N., Maruyama, N., Terada, S., Kojima, M., Sakakibara, H., and Okada, K. (2015). CLUMSY VEIN, the Arabidopsis DEAH-box Prp16 ortholog, is required for auxin-mediated development. Plant J 81, 183-197.
- Verma, A., Lee, C., Morriss, S., Odu, F., Kenning, C., Rizzo, N., Spollen, W.G., Lin, M., McRae, A.G., Givan, S.A., Hewezi, T., Hussey, R., Davis, E.L., Baum, T.J., and Mitchum, M.G. (2018). The novel cyst nematode effector protein 30D08 targets host nuclear functions to alter gene expression in feeding sites. New Phytol 219, 697-713.
- Vijayakumari, D., Sharma, A.K., Bawa, P.S., Kumar, R., Srinivasan, S., and Vijayraghavan, U. (2019). Early splicing functions of fission yeast Prp16 and its unexpected requirement for gene Silencing is governed by intronic features. RNA Biol 16, 754-769.
- Wang, H.L., Zhang, Y., Wang, T., Yang, Q., Yang, Y., Li, Z., Li, B., Wen, X., Li, W., Yin, W., Xia, X., Guo, H., and Li, Z. (2021). An alternative splicing variant of PtRD26 delays leaf senescence by regulating multiple NAC transcription factors in Populus. Plant Cell 33, 1594-1614.
- Wang, Y., Wagner, J.D., and Guthrie, C. (1998). The DEAH-box splicing factor Prp16 unwinds RNA duplexes in vitro. Curr Biol 8, 441-451.

- Wilkinson, M.E., Charenton, C., and Nagai, K. (2020). RNA Splicing by the Spliceosome.

 Annu Rev Biochem 89, 359-388.
- Wong, J.J., Ritchie, W., Ebner, O.A., Selbach, M., Wong, J.W., Huang, Y., Gao, D., Pinello, N., Gonzalez, M., Baidya, K., Thoeng, A., Khoo, T.L., Bailey, C.G., Holst, J., and Rasko, J.E. (2013). Orchestrated intron retention regulates normal granulocyte differentiation. Cell 154, 583-595.
- Wu-Scharf, D., Jeong, B., Zhang, C., and Cerutti, H. (2000). Transgene and transposon silencing in Chlamydomonas reinhardtii by a DEAH-box RNA helicase. Science 290, 1159-1162.
- Xu, F., Xu, S., Wiermer, M., Zhang, Y., and Li, X. (2012). The cyclin L homolog MOS12 and the MOS4-associated complex are required for the proper splicing of plant resistance genes. Plant J 70, 916-928.
- Yang, S., Gao, M., Xu, C., Gao, J., Deshpande, S., Lin, S., Roe, B.A., and Zhu, H. (2008). Alfalfa benefits from Medicago truncatula: the RCT1 gene from M. truncatula confers broad-spectrum resistance to anthracnose in alfalfa. Proc Natl Acad Sci U S A 105, 12164-12169.
- Zhan, X., Yan, C., Zhang, X., Lei, J., and Shi, Y. (2018). Structure of a human catalytic step I spliceosome. Science 359, 537-545.
- Zhang, P., Jia, Y., Shi, J., Chen, C., Ye, W., Wang, Y., Ma, W., and Qiao, Y. (2019). The WY domain in the Phytophthora effector PSR1 is required for infection and RNA silencing suppression activity. New Phytol 223, 839-852.
- **Zhang, X.C., and Gassmann, W.** (2003). RPS4-mediated disease resistance requires the combined presence of RPS4 transcripts with full-length and truncated open reading frames. Plant Cell **15**, 2333-2342.
- Zhang, Z., Liu, Y., Ding, P., Li, Y., Kong, Q., and Zhang, Y. (2014). Splicing of receptor-like kinase-encoding SNC4 and CERK1 is regulated by two conserved splicing factors that are required for plant immunity. Mol Plant 7, 1766-1775.

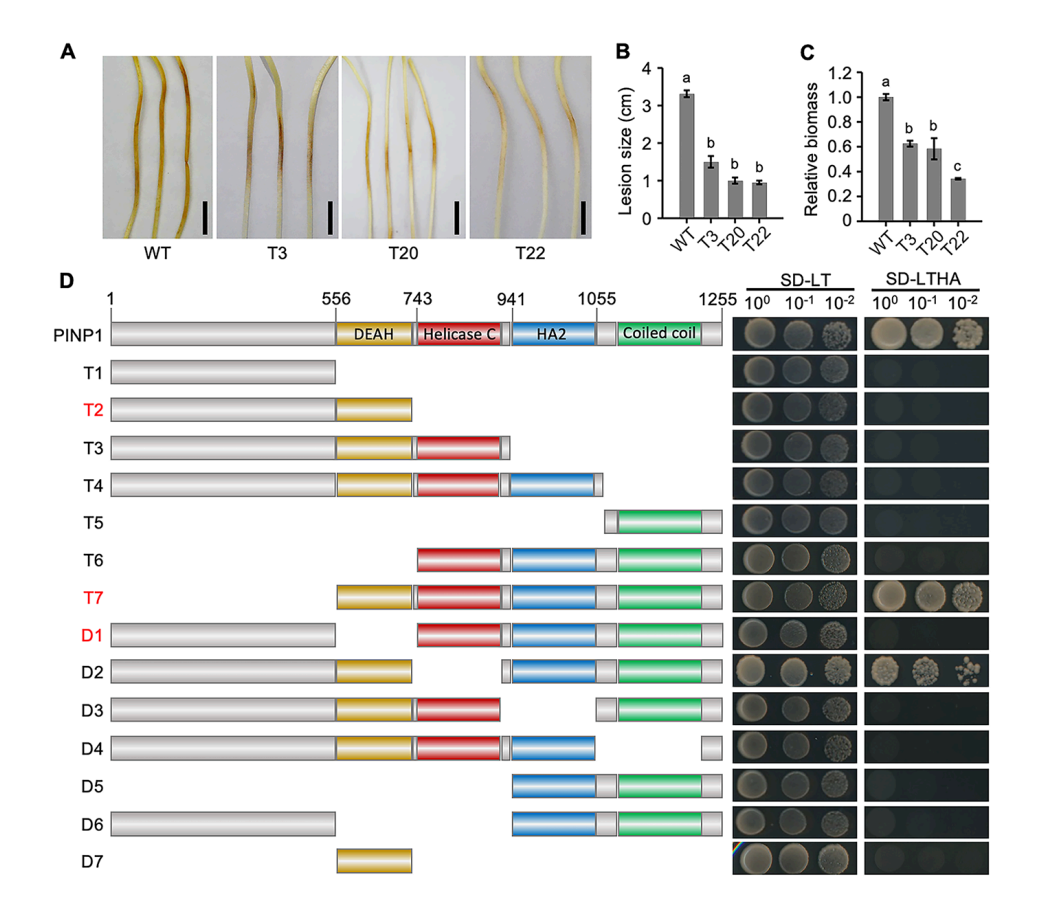


Figure 1 PSR1 contributes to the pathogenicity of *P. sojae* and binds to the conserved C-terminus of PINP1.

- **(A)** Knocking out *PSR1* in *P. sojae* significantly reduced infection in soybean hypocotyls. Disease symptoms were monitored in etiolated hypocotyls of three *PSR1*-edited transformants (T3, T20, T22). Photos were taken at 7 dpi. Bars = 1 cm.
- **(B)** Analysis of lesion size in soybean hypocotyls. Data in (B) and (C) represent means \pm standard error (SE). Different letters indicate statistically significant differences among samples (P < 0.01; Duncan's multiple range test, Supplemental File 1). Experiments were repeated twice with similar results.
- **(C)** Quantification of *P. sojae* biomass in soybean hypocotyls by genomic DNA-based quantitative PCR (qPCR). Experiments were repeated twice with similar results.
- **(D)** Schematic representation of various *PINP1* truncation and deletion constructs (left) examined in yeast two-hybrid (Y2H) assays (right). Yeast cells were transformed with pGBKT7 (DNA-binding domain plasmid carrying *PSR1* as bait), together with pGADT7 (activation domain plasmid carrying various *PINP1* derivates as prey). Transformants were selected on minimal medium (SD/–Leu–Trp (–LT) and SD/–Leu–Trp–His–Ade (–LTHA). The ability of yeast colonies to grow on –LTHA plates indicates an interaction between the two proteins.

The experiment was performed twice with similar results. DEAH, Asp-Glu-Ala-His; HA2 helicase-associated domain 2.

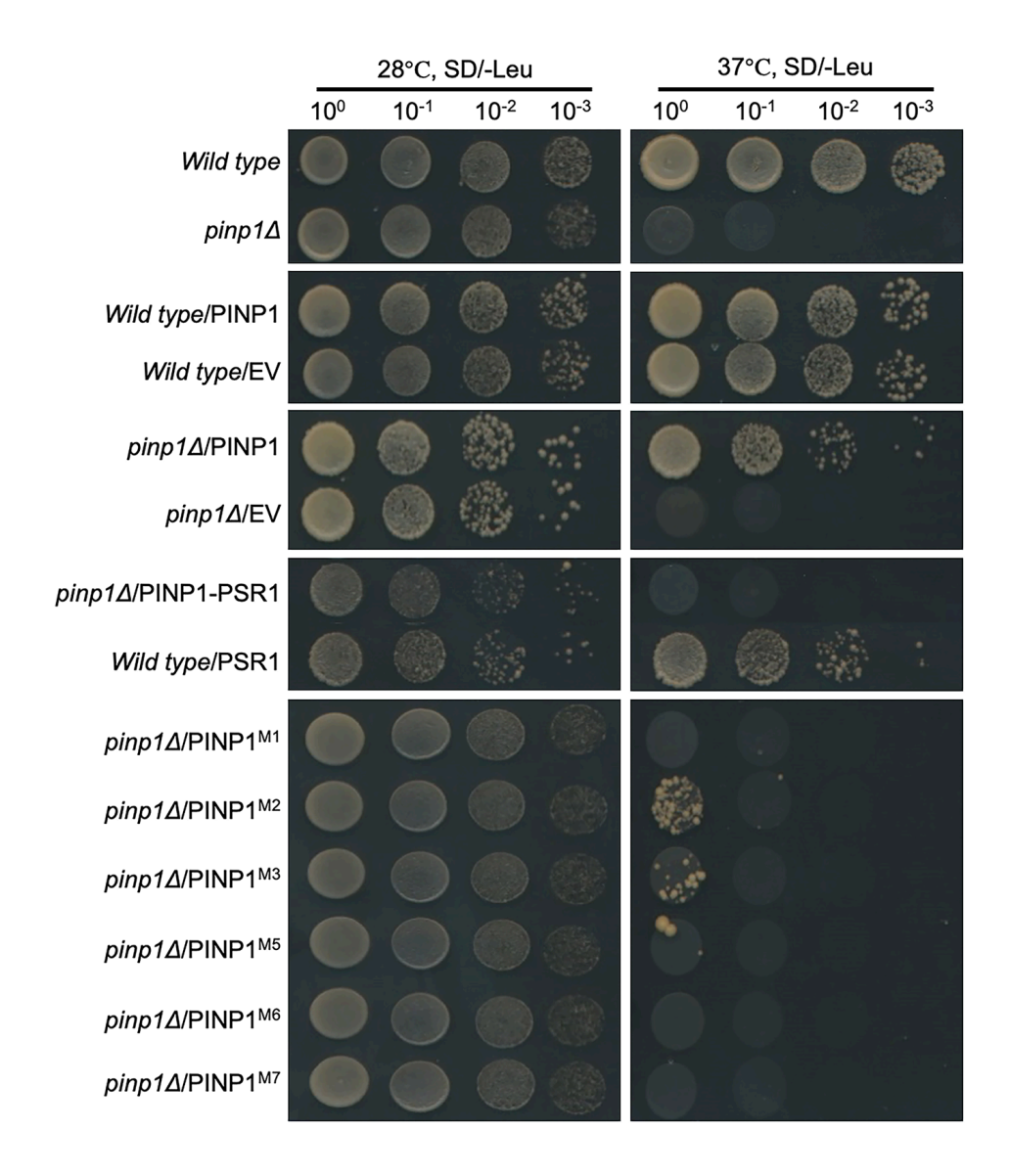


Figure 2 Complementation assay using the yeast temperature-sensitive $pinp1\Delta$ mutant. The $pinp1\Delta$ yeast strain was transformed with EV (empty vector control), PSR1, PINP1, and/or PINP1 derivates. The transformants were plated on minimal medium (SD/–Leu) in which glucose was replaced with an equal amount of galactose as the carbon source and incubated at

28°C (left) and 37°C (right) for 72 h. PSR1 blocks the ability of *Arabidopsis* PINP1 to complement the growth phenotype of the temperature-sensitive yeast $pinp1\Delta$ mutant. The wild-type yeast strain was used as a positive control. Experiments were repeated twice with similar results.

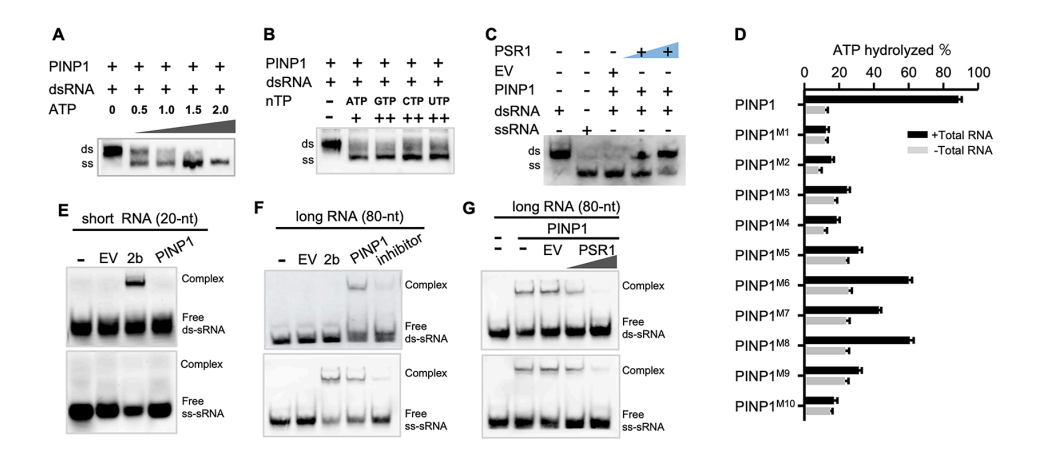


Figure 3 PSR1 reduces both the RNA unwinding and RNA-binding activities of PINP1 in vitro.

- (A) PINP1 exhibits ATP-dependent double-stranded RNA (dsRNA) unwinding activity.
- **(B)** PINP1 can utilize CTP, UTP, and GTP in addition to ATP as energy sources to drive the helicase reaction.
- **(C)** EMSA showing that PSR1 hinders the dsRNA unwinding activity of the PINP1protein. The blue color represents an increasing amount of PSR.
- **(D)** ATP hydrolysis by wild type (WT) and mutant PINP1 proteins. The ATPase activity of WT PINP1 and ten different PNIP1 mutants was measured in the presence and absence of total RNA extracted from *Arabidopsis*. Data in (D) represent means \pm SE. Experiments were repeated twice with similar results.
- (**E** and **F**) Electrophoretic mobility shift assays (EMSAs) showing that PINP1 does not bind to short (20-nt) single-stranded RNA (ssRNA) and dsRNA (**E**) but binds to long (80-nt) ssRNA and dsRNA (**F**). The viral RNA silencing suppressor 2b, which binds to short dsRNA, was used as a positive control.
- **(G)** EMSA showing that PSR1 affects the RNA-binding activity of PINP1. Experiments were repeated twice with similar results.

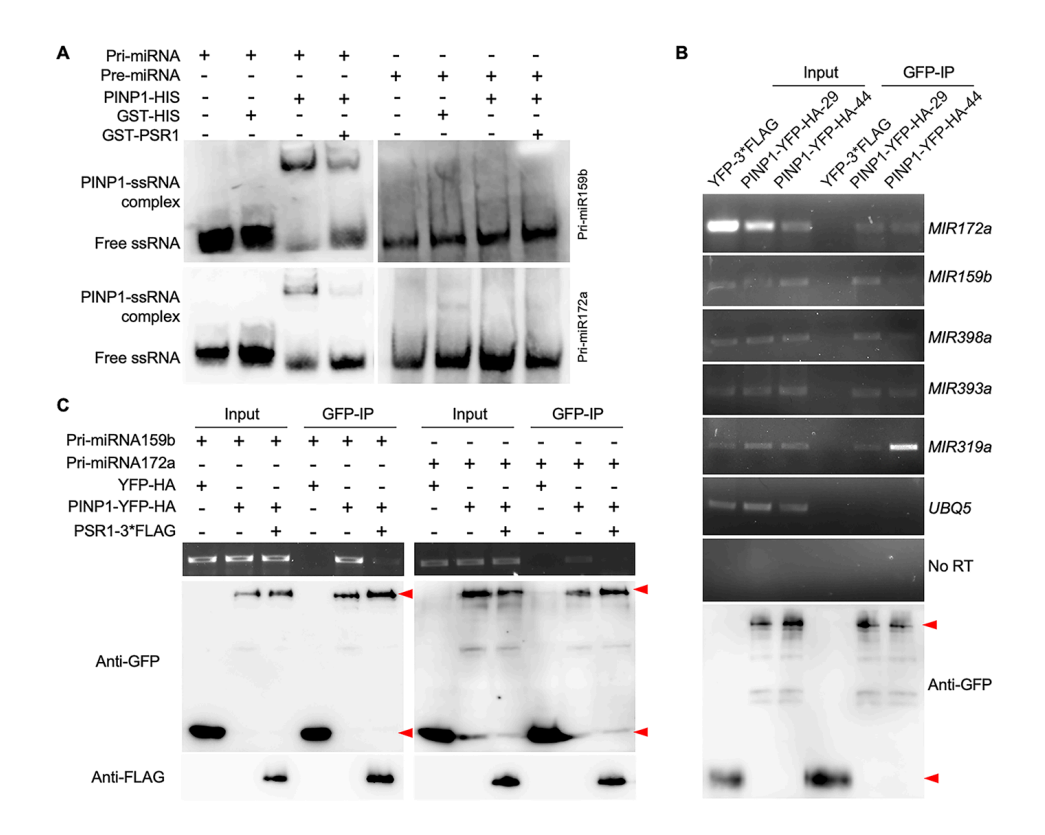


Figure 4 PSR1 interferes with the binding of PINP1 to pri-miRNAs in vitro and in vivo.

- **(A)** EMSA to determine potential binding of PINP1 to pri-miRNAs (left panel) and pre-miRNAs (right panel). GST-HIS, GST-PSR1, and PINP1-HIS recombinant proteins were expressed in *E. coli*. The biotin-labeled synthetic pri/pre-miRNA fragments were incubated with the purified PINP1-HIS, GST-PSR1, or GST-HIS protein.
- **(B)** PINP1 binds pri-miRNAs *in vivo* as detected by RNA immunoprecipitation assay (RIP). Arabidopsis leaves from transgenic YFP-FLAG and PINP1-YFP-HA lines were used for RIP assays with GFP beads. YFP-FLAG was used as a negative control. Five percent of IPs and 10% input proteins were used for immunoblotting. *UBQ5* was used as an internal control, no RT was used as a negative control.
- (C) PSR1 impairs the interaction of PINP1 with pri-miRNA159b (left panel) and pri-miRNA172a (right panel). The RIP assay was performed by transiently co-expressing PINP1-YFP-HA and individual pri-miRNA constructs together with or without PSR1 constructs in N. benthamiana leaves. After 48 h post-infiltration, leaf tissues were sampled and used for RIP analysis with GFP beads. Experiments were repeated twice with similar results.

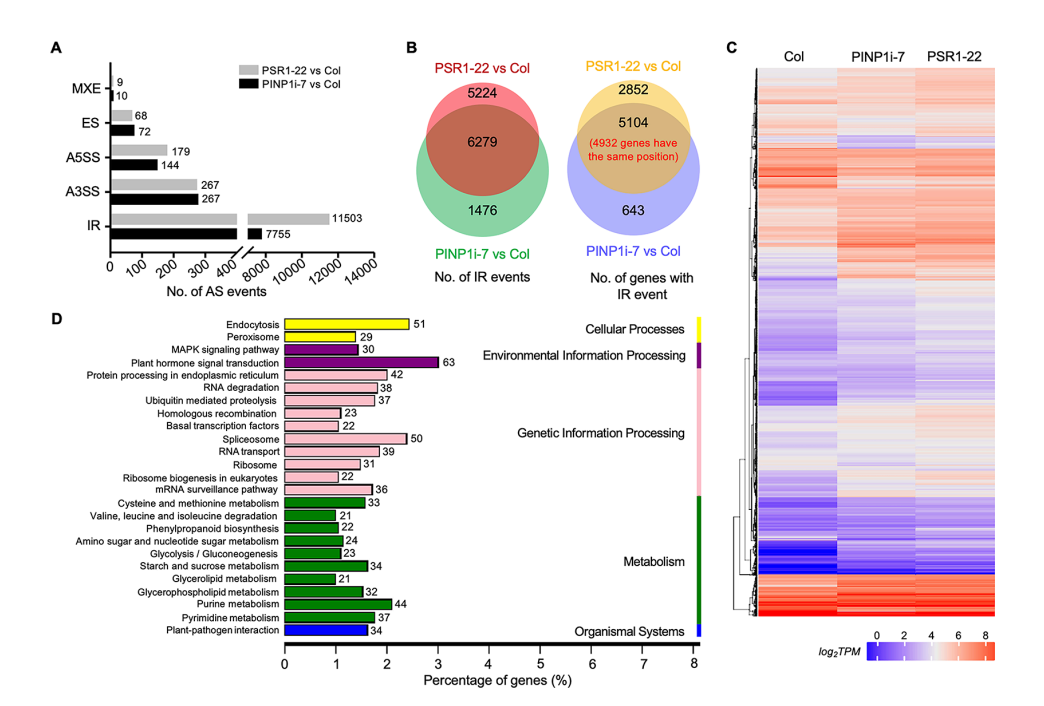


Figure 5 The effects of PSR1 on alternative splicing (AS) are dependent on PINP1 splicing activity.

- (A) Number of different types of AS events identified in PSR1 overexpression line (PSR1-22, grey) and PINP1-silenced line (PINP1i-7, black) vs WT Arabidopsis (Col). The AS events in two samples were categorized into five major AS types: MXE, mutually exclusive exons; ES, exon skipping; A5SS, alternative 5' splice site; A3SS, alternative 3' splice site; IR, intron retention.
- **(B)** Venn diagrams indicating the number of overlapping IR events (left) and genes (right) in PSR1-22 and PINP1i-7 vs. WT (Col). A total of 6,279 IR events (the most abundant AS event) were common to both PSR1-22 and PINP1i-7 genotypes.
- **(C)** Heat map showing the RNA-seq read count (transcripts per million [TPM]) for differential IR events (corresponding to 5,104 genes) in PSR1-22 and PINP1i-7 plants. TPM, Transcripts per million.
- **(D)** Gene Ontology enrichment analysis of genes with differential AS events in PSR1-22 and PINP1i-7 plants

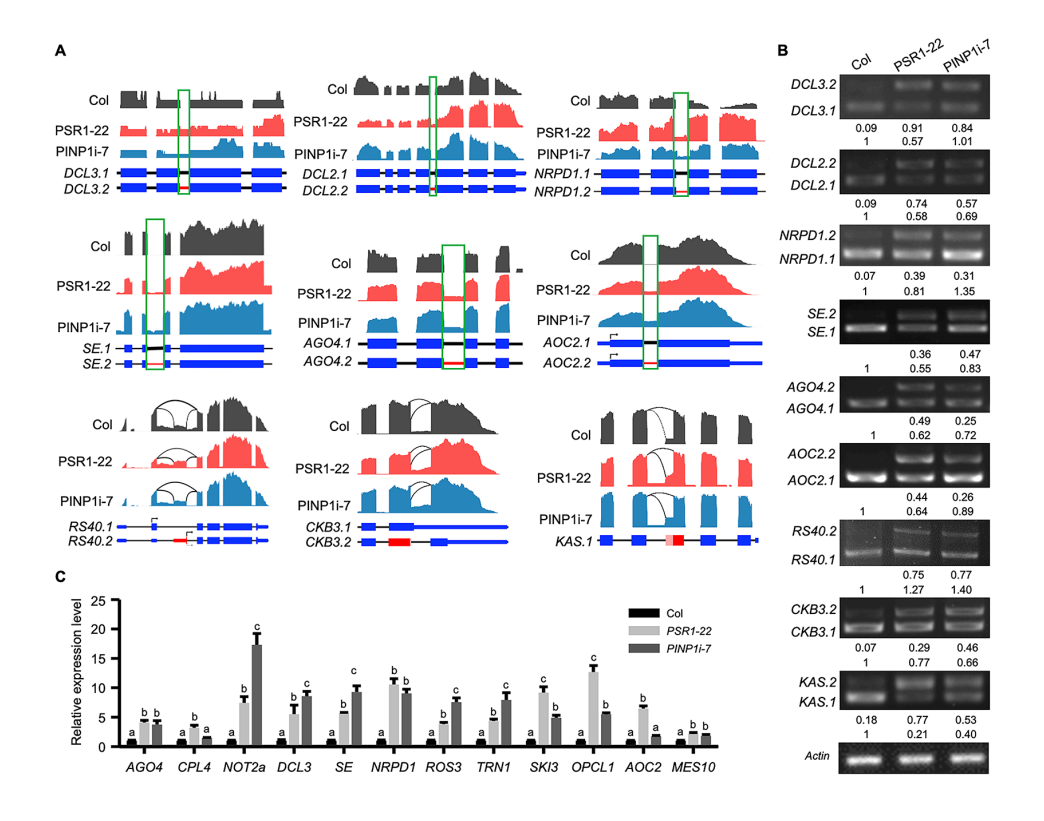


Figure 6 Validation of AS predictions by RNA-seq and RT-PCR.

- (A) Nine examples of mRNAs with splicing defects (6 IR, 1 ES, 1 A5SS, and 1 A3SS events), as detected by RNA-seq. Wiggle plots showing the normalized read coverage data on a logarithmic scale (log2) for Col-0 (Col; grey), PSR1-22 (pink), and PINP1i-7 (light blue) and lines with splicing defects (dark blue). Green frames indicate splicing defects. Diagrams of annotated gene structures are shown at the bottom, showing exons (light blue boxes) and introns (black lines. The red lines and boxes represent splicing defects.
- **(B)** Validation of AS events in the corresponding nine genes by RT-PCR. Upper and lower bands represent the unspliced and spliced forms of mRNAs, respectively.
- (C) Real-time RT-PCR analysis of 12 intron-retaining gene transcripts in Col-0 (Col, black), PSR1-22 (light grey), and PINP1i-7 (dark grey) plants. AtActin1 was used as the internal standard. Data represent means \pm SE. Different lowercase letters represent statistically significant differences (P < 0.01; Duncan's multiple range test, Supplemental File 1). The experiments were repeated twice with similar results.

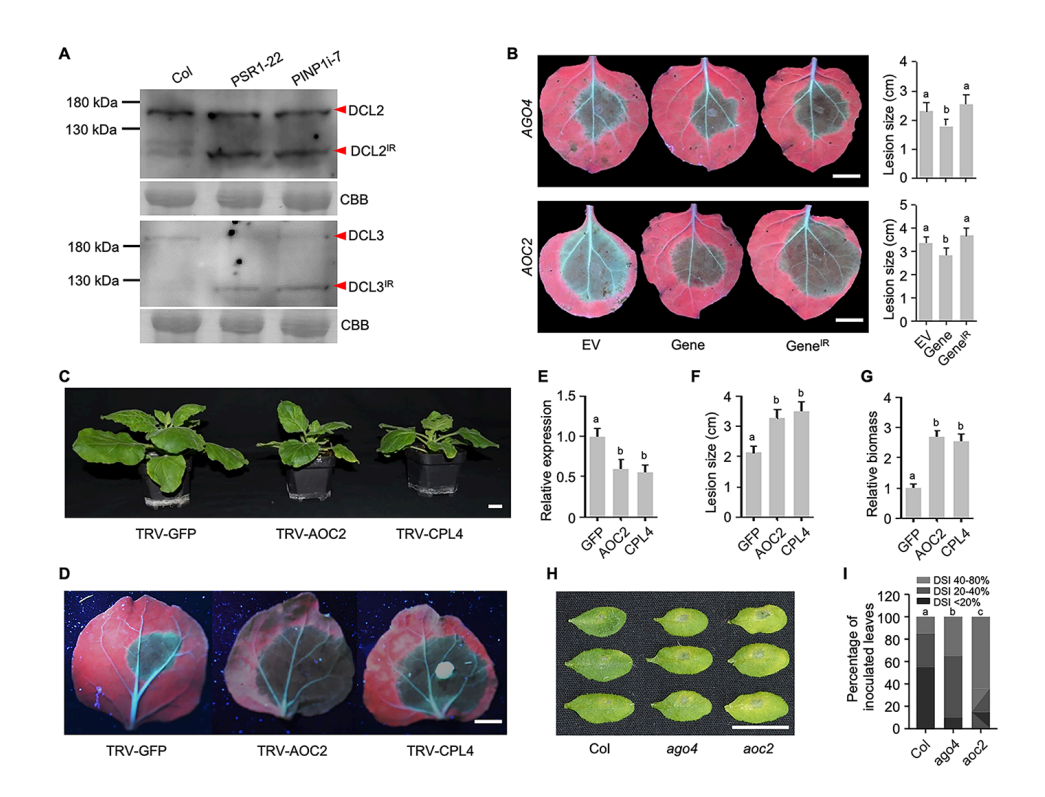


Figure 7 Expression of intron-retaining genes enhances host susceptibility to *Phytophthora* infection in *N. benthamiana*.

- (A) Immunoblot analysis of full-length and truncated protein expression in WT Col-0 (Col), PSR1-22, and PINP1i-7 plants using anti-DCL2- (upper panel) and anti-DCL3- (lower panel) specific antibodies. Coomassie brilliant blue (CBB) staining was used as a loading control for immunoblot analyses
- **(B)** Disease symptoms (left) and lesion size (right) of different isoforms of AGO4 and AOC2 genes involved in plant defense against *Phytophthora parasitica* infection. Pathogen inoculation assays show that all genes tested were positive regulators of plant immunity against *P. parasitica*. *N. benthamiana* leaves were infiltrated with *Agrobacterium tumefaciens* carrying GFP or different IR genes. The infiltrated areas of leaves were inoculated with P. parasitica zoospores at 24 hpi. Lesion size was measured at 48 hpi. EV, empty vector. Bar = 10 mm.
- (C) Side view of 3–4-week-old plants inoculated with control (TRV:GFP), AOC2 (TRV:AOC2), or CPL4 (TRV:CPL4) silencing vectors. Bar = 10 mm.
- **(D)** Disease symptoms of AOC2- or CPL4-silenced N. benthamiana leaves challenged with P. capsici. Bar = 10 mm.
- **(E)** Relative transcript levels of *AOC2* and *CPL4* genes in individual gene-silenced leaves of *N. benthamiana*. RNA samples were isolated from leaves co-infiltrated with TRV1 and TRV2:GFP, TRV2:AOC2, or TRV2:CPL4. The *Actin* gene from *N. benthamiana* was used as an internal control.
- **(F)** Statistical analysis of lesion length.
- **(G)** Relative biomass of P. capsici, as determined by qPCR.

- (H) Disease symptoms of leaves (n = 55 leaves) in loss-of-function *ago4* and *aoc2* mutants upon *P. capsici* infection. Leaves were photographed under white light at 48 hpi. Bar = 10 mm. (I) Quantitative analysis of disease severity. (different letters indicate statistically significant differences based on the Wilcoxon rank-sum test).
- In (B) and (E–G), data represent means \pm SE. Different lowercase letters represent statistically significant differences (P < 0.01; Duncan's multiple range test, Supplemental File 1). These experiments were repeated in triplicates with similar results.

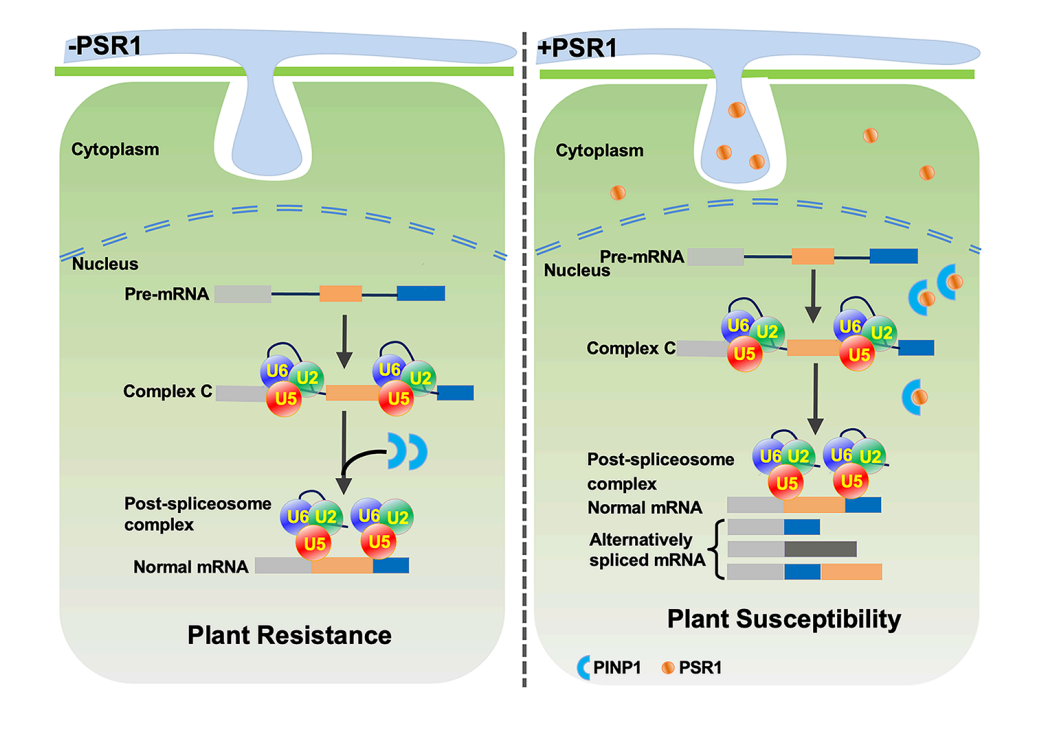


Figure 8 Model displaying the role of PSR1–PINP1 interaction in sRNA biogenesis and plant defense response.

In the absence of the PSR1 effector (left), PINP1 is the key spliceosome component, which regulates the second step of pre-mRNA splicing by promoting a conformational change of the spliceosome. Proper splicing of sRNA related genes and pathogenesis related (PR) genes contribute to disease resistance. In the presence of the PSR1 effector (right), PINP1 associates with PSR1 in the nucleus. Reduction in the PINP1 protein level results in large-scale production of unspliced and abnormally spliced mRNA isoforms and the inhibition of PINP1 binding to pri-miRNAs, thereby regulating the host splicing machinery to suppress sRNA biogenesis and plant immunity.